Characterization of pyridomycin B reveals the formation of functional groups in antimycobacterial pyridomycin

1   Tingting Huang[*], Zihua Zhou, Maolong Wei, Lin Chen, Zhihong Xiao, Zixing Deng, Shuangjun Lin

2

3

4   **Affiliations**

5   State Key Laboratory of Microbial Metabolism, and Joint International Research Laboratory on

6   Metabolic& Developmental Sciences, and School of Life Sciences & Biotechnology, Shanghai Jiao

7   Tong University, Shanghai, 200240, China

8

9   ***** Address correspondence to Tingting Huang, tingwing82@sjtu.edu.cn

10   **Keywords**: pyridomycin, antimycobacterial activity, biosynthesis, enoyl ester, trans ketoreductase

11   **Running title**: Characterization of the new pyridomycin analogue

12

Abstract

Pyridomycin, a cyclodepsipeptide with potent antimycobacterial activity, specifically inhibits the InhA enoyl reductase of *Mycobacteria tuberculosis*. Structure-activity relationship studies indicated that the enolic acid moiety in pyridomycin core system is an important pharmacophoric group and the natural configuration of the C-10 hydroxyl contributes to the bioactivity of pyridomycin. The ring structure of pyridomycin was generated by the nonribosomal peptide synthetase (NRPS) and polyketide synthase (PKS) hybrid system (PyrE-F-G). Bioinformatics analysis reveals that SDR family protein Pyr2 functions as a 3-oxoacyl ACP reductase in the pyridomycin pathway. Inactivation of *pyr2* resulted in accumulation of pyridomycin B, a new pyridomycin analogue featured with enol moiety in pyridyl alanine moiety and a saturated 3-methylvaleric acid group. The elucidated structure of pyridomycin B suggests that rather than functioning as a post-tailoring enzyme, Pyr2 catalyzes ketoreduction to form the C-10 hydroxyl group in pyridyl alanine moiety and the double bond formation of the enolic acid moiety derived from isoleucine when the intermediate assembled by PKS-NRPS machinery is still tethered to the last NRPS module, in a special energy-saving manner. Ser-His-Lys residues constitute the active site of Pyr2, which is different from the typically conserved Tyr based catalytic triad in the majority of SDRs. Site-directed mutation identified that His154 in the active site is a critical residue for pyridomycin B production. These findings will improve our understanding of the pyridomycin biosynthetic logic, identify the missing link for the double bound formation of enol ester in pyridomycin and enable creating chemical diversity of pyridomycin derivatives.

Importance

Tuberculosis (TB) is one of the world's leading causes of death by infection. Recently, pyridomycin, the antituberculous natural product from Streptomyces has garnered considerable attention for being

37 determined as a target inhibitor of InhA enoyl reductase of *Mycobacteria tuberculosis*. In this study,

38 we report a new pyridomycin analogue from mutant HTT12, demonstrate the essential role of a

39 previously ignored gene *pyr2* in pyridomycin biosynthetic pathway, and imply that Pyr2 functions as

40 a *trans* ketoreductase (KR) contributing to the formation of functional groups of pyridomycin utilize

41 a distinct catalytic mechanism. As enol moiety are important for pharmaceutical activities of

42 pyridomycin, our work would expand the understanding the mechanism of SDR family proteins and

43 set the stage for future bioengineering of new pyridomycin derivatives.

44

45

Introduction

Tuberculosis (TB) remains a major global health problem, causing an estimated 10.0-million people developed TB disease in 2017 (1). With the appearance of multidrug-resistant strains of TB to all the antitubercular chemotherapies, more efficient TB control call for the development of new antimycobacterial drugs. Classic biochemical approaches, '-omics' technologies including genomic- and proteomic-based approaches combined with computational chemistry strategies allow target discovery of natural products with antimycobacterial activity (2-4). Recently, reappraisal of known natural products becomes a research strategy to accelerate the development of antimycobacterial drug leads from natural products (5, 6). In *Mycobacteria tuberculosis* (*Mtb*), InhA is an NADPH-dependent enoyl-acyl carrier protein (ACP) reductase from the FASII pathway essential for synthesizing mycolic acids of cell wall (7, 8). The clinical TB drugs isoniazid and ethionamide are prodrugs that are activated by the catalase-peroxidase KatG of *Mtb* to form an adduct with NAD^+ and then target the substrate-binding site of InhA (9). In the aim of finding new antimycobacterial compounds, pyridomycin has been identified as an InhA competitive inhibitor (10).

Pyridomycin (Figure 1A, **1**) is a cyclodepsipeptide produced by *Streptomyces pyridomyceticus* NRRL B-2517 (11). The 12-membered core ring is composed of two pyridyl groups (a N-3-hydroxypicolinyl-L-threonine and a 3-(3-pyridyl)-L-alanine), a propionic acid, and a structurally unique 2-hydroxy-3-methylpent-2-enoic acid (12). From the X-ray crystallography of pyridomycin-InhA complex, the two pyridyl groups of pyridomycin occupy the NADPH cofactor binding site of InhA, and the enolic acid (2-butan-2-ylidene) moiety protrudes into the lipid substrate binding pocket. The unique configuration that simultaneously spans both the cofactor and the substrate-binding pocket of InhA endows pyridomycin with potent activity against InhA-resistant strains of *Mtb* (10, 13).

69   Further structure-activity relationship (SAR) investigation of chemical synthesized

70   dihydropyridomycins (Figure 1A, **2** and **3**) revealed that substitution of the enolic acid moiety of

71   pyridomycin by 2*R*-isopropyl moiety (**2**) made the compound less active (four-fold lower than

72   pyridomycin) while the substitution with a 2*S*-isopropyl residue (**3**) led to diminished activity

73   compared to pyridomycin (14). Meanwhile, the hydroxyl group on C-10 is an essential stereocenter

74   for pyridomycin activity (15). Until now, only one total synthesis of pyridomycin has been reported

75   (16) and the establishment of enolic acid moiety was one of the major difficulties. Motivated by the

76   promising activity and the structural uniqueness, we set out to decipher the biosynthesis of

77   pyridomycin both at the genetic and the biochemical level.

78   Nonribosomal peptide synthetases (NRPSs) and polyketide synthases (PKSs) multifunctional

79   enzyme complexes composed of successive catalytic domains that are themselves coordinated

80   organized into biosynthetic modules. Each module in the assembly line performs iterative chemical

81   reactions to produce numerous natural products (17). In contrast to the co-linear manner of PKSs or

82   NRPSs, a growing number of trans-acting units has been identified, including trans-acyltransferase

83   (AT) for loading PKS building blocks, trans-enoylreductases (ER) for reduction of α,β-unsaturated

84   intermediates, and trans-ketoreductase (KR) to reduce a β-ketone to a hydroxyl group (18-23).

85   Previous biosynthetic studies showed that the pyridomycin core structure was assembled by a hybrid

86   NRPS-PKS system consisting of PyrA, PyrU, PyrE, PyrF, and PyrG. Among them, PyrA (AMP

87   ligase) and PyrU (peptidyl carrier protein, PCP) functioned as a free-standing adenylation (A)

88   domain and a PCP respectively, which formed the loading module to activate and load starter unit 3-

89   HPA (3-Hydroxy pyridine carboxylic acid) (24). PyrE, F, G encode NRPS-PKS proteins comprising

90   four modules in total. PyrE is a typical NRPS dimodule consisting of two minimal NRPS modules

91   (C-A-PCP) that are predicted to sequentially incorporate threonine and 3-(3-pyridyl)-L-alanine. PyrF

92   is the sole PKS module (KS-AT-MT-ACP) and was believed to incorporate propionic acid into the

93   pyridomycin backbone. PyrG is a special NRPS module, which contains two tandem A domains and

94   a PKS-type ketoreductase (KR) domain (25). The second A domain in PyrG was functional for

95   recoganization and activation of α-keto-β-methylvaleric acid (2-KVC) as the native substrate. The

96   KR domain of PyrG further catalyzed the reduction of the 2-KVC tethered onto the PCP of PyrG to

97   generate the PCP-tethered α-hydroxy-β-methylvaleric acid (2-HVC). A biosynthetic pathway has

98   been proposed for the pyridomycin core structure based on these PKS/NRPS related enzymes (24). In

99   addition, there are some other genes in the cluster with yet unassigned biosynthetic functions, which

100   might be involved in the modification step during or after the NRPS/PKS process.

101   Intriguingly, according to pyridomycin structure, no KR domain was found in PyrF which was

102   thought to be responsible for the reduction of the β-keto group to form the hydroxyl group (*).

103   Besides, little was known about the formation of double bond of the enolic acid moiety. Close

104   inspection of the pyridomycin gene cluster showed that *pyr2* encodes a 3-oxoacyl-acyl-carrier-protein

105   (ACP) ketoreductase that is highly homologous to FabG from the bacterial type II fatty acid synthase.

106   FabG is a member of the ketoacyl reductase family of proteins and is an essential enzyme for type II

107   fatty acid biosynthesis that catalyzes an NADPH-dependent reduction of β-ketoacyl-ACP to the β-

108   hydroxyacyl isomer, which is the first reductive step in the elongation cycle of fatty acid

109   biosynthesis. We speculate that Pyr2, a 3-ketoacyl-ACP reductase may act as a freestanding

110   ketoreductase in a similar manner as FabG, to reduce the β-ketoacyl intermediates tethered to PyrF-

111   ACP (Figure 1B). By using gene inactivation and complementation, we identified *pyr2* as an

112   essential gene for pyridomycin biosynthesis; isolation and characterization of the resulting new

113   pyridomycin derivative from the *pyr2* mutant shed new insight into the biosynthesis of functional

114   groups in pyridomycin. Our study not only confirmed a trans-acting NRPS/PKS specific tailoring

115   enzyme creating chemical diversity of pyridomycin, but also provides the opportunity to explore the

116   biosynthetic mechanism of functional moieties in pyridomycin.

117

Results

Bioinformatics analysis of Pyr2

120 *Pyr2*, encoding a 3-ketoacyl-acyl-carrier protein reductase, located upstream of pyridomycin NRPS-
121 PKS genes which was originally identified as the boundary of pyridomycin gene cluster (24). Pyr2
122 belongs to the short-chain dehydrogenase/reductases (SDR) super family oxidoredutase with
123 significant sequence identity (~50%) (26, 27). The amino acid sequence of Pyr2 was blast searched in
124 microbial genome database and compared for its similarity. It reveals that Pyr2 shares sequence
125 homology with 3-oxoacyl-ACP reductase from *Streptomyces gancidicus* (58% identity and 70%
126 similarity) or from *Allonocardiopsis opalescens* (57% identity and 72% similarity). A database
127 search of Pyr2 revealed homologs from various microorganisms, mostly are from high GC gram-
128 positive strains in the phylogenetic survey. A sequence similarity network of Pyr2 with its homologs
129 found at an e-value threshold of 10^{-80} was established (Figure 2). In the type II FAS system, 3-
130 oxoacyl-ACP reductase catalyzes the first reduction step that leads to the conversion of 3-oxoacyl-
131 ACP to 3-D-hydroxyacyl-ACP intermediate during the elongation cycle. Therefore, Pyr2 was
132 considered as the most likely candidate to catalyze the C-10-keto reduction step in pyridomycin
133 biosynthesis.

Inactivation and Functional Complementation of *pyr2*

135 To assess the necessary of *pyr2* for pyridomycin production, gene inactivation was achieved
136 through substituting *pyr2* by the kanamycin resistance cassette using the λ_{RED}-mediated PCR-
137 targeting mutagenesis. The resultant double-crossover mutant *S. pyridomyceticus* HTT-12 was
138 confirmed and its fermentation profile was detected by HPLC-MS (24). The mutant HTT12 retained
139 the ability to produce a peak with the similar retention time (~16.4 min) to that of pyridomycin on

140   HPLC profile, exhibiting a molecular ion peak at m/z 541 $[M + H]^+$ same as that of pyridomycin

141   (Figure 3A). The crude extracts of *S. pyridomyceticus* and HTT12 mutant were tested for

142   antimycobacterial activity using a standard disk diffusion assay. Both of them showed similar

143   inhibition zone on the bioassay agar plate (Figure 3B and 3C) which seems that *pyr2* is not included

144   within the pyridomycin biosynthetic gene cluster (24).

145   Surprisingly, although the molecular weight of the product from HTT12 is as the same as that of

146   the pyridomycin, the peak from HTT12 does not show a higher absorption shoulder at around 230 nm

147   from the UV/Vis spectroscopy, which is slightly different from the UV/Vis spectrum feature of

148   pyridomycin (Figure 3B and 3C). A closer inspection and comparison of the LC-MS/MS profile

149   revealed that they had different MS/MS patterns (Figure 3E and 3F). Analysis of the peak from

150   HTT12 in positive-ion mode showed a MS/MS fragmentation pattern (m/z 205.0, 409.1, and 427.1

151   for $[M + H]^+$), presenting a -2 mass shift, compared to the fragmentation data (m/z 207.1, 411.1, and

152   429.1 for $[M + H]^+$) of pyridomycin. Additionally, the two profiles also share the same ion peaks

153   such as m/z at 223.0 $[M + H]^+$ and 337.0 $[M + H]^+$. The assignment of these fragmental ions based on

154   the MS/MS2 data suggests that the peak in HTT12 contains a partial structure of pyridomycin and

155   these fragments with modification on 3-(3-pyridyl)-L-alanine moiety.

156   To test whether the retention time shift and MS/MS pattern variation in HTT12 were actually

157   caused by the *in vivo* deletion of *pyr2*, a complementation experiment was carried out through

158   introduction of the integrative vector pJTU4656, a shuttle plasmid harboring a copy of *pyr2* under the

159   control of the strong promoter *PermE**, into the Δ*pyr2* mutant HTT12 through conjugation.

160   HTT12/pJTU4656 was selected in the presence of both apramycin and kanamycin. Subsequently, the

161   culture extracts from the complementation strain were analyzed by HPLC-MS (Figure 3A, lane c).

162   Although it was relatively less than the wild type strain, the peak in HTT12/pJTU4656 showed same

163   MS/MS pattern as pyridomycin, indicating that pyridomycin production was restored with intact *pyr2*

164 complementation. Taken together, the requirement of *pyr2* in the biosynthesis of pyridomycin was

165 supported by *pyr2* inactivation and complementation. Pyr2 should play a specific role in the

166 biosynthesis of pyridomycin.

Isolation and structure elucidation of pyridomycin analogue from Δ*pyr2* mutant HTT12

168 The differences in the MS/MS patterns of the peak from Δ*pyr2* mutant HTT12 and wild type

169 producer encouraged a large-scale fermentation to isolate the pyridomycin related compound.

170 Following previous reported procedures (24), a 19-L culture of the mutant HTT12 was subjected for

171 ethyl acetate extraction and subsequent column chromatography resulted in the isolation of

172 compound **HTT12-1**.

173 **HTT12-1** was isolated as a white powder. The molecular formula $C_{27}H_{32}N_4O_8$ was established

174 based on its HR-MS data at *m/z* 541.2291 (calcd. 541.2293 for $[M + H]^+$), requiring 14 degrees of

175 unsaturation (DOUs). The ^{1}H NMR data of **HTT12-1** showed signals for four methyl groups [δ_H 0.96

176 (3H, t, *J* = 7.5 Hz), 1.00 (3H, d, *J* = 7.0 Hz), 1.38 (3H, d, *J* = 7.0 Hz) and 1.53 (3H, s)], four

177 oxygenated or nitrogenated methines [δ_H 4.06 (1H, d, *J* = 4.5 Hz), 4.61 (1H, brs), 5.57 (1H, m) and

178 5.88 (1H, d, *J* = 1.5 Hz)], a 2,3-disubstituted pyridine unit [δ_H 8.19 (1H, d, *J* = 4.3 Hz), 7.51 (1H, dd,

179 *J* = 8.5, 4.3 Hz) and 7.41 (1H, d, *J* = 8.5 Hz)], a *meta*-disubstituted pyridine moiety [δ_H 8.39 (1H, dd,

180 *J* = 4.8, 1.3 Hz), 8.22 (1H, d, *J* = 1.3 Hz), 7.56 (1H, d, *J* = 7.7 Hz) and 7.34 (1H, d, *J* = 7.7, 4.8 Hz)]

181 and a series of aliphatic multiplets. The ^{13}C NMR spectrum, in combination with HSQC experiment

182 resolved 27 carbon resonances consistent with four methyls, two *sp³* methylenes, one *sp³* methine,

183 four oxygenated or nitrogenated *sp³* tertiary carbons, a tetrasubstituted double bond, two pyridine

184 units, and four ester or amide carbonyl groups. As 13 of the 14 DOUs were attributed to two pyridine

185 units, a double bond and four carbonyl groups, the remaining for DOUs required for **HTT12-1** was

186   monocycle. The aforementioned data were similar to the pyridomycin (1), except for the absence of

187     $\Delta^{2,1'}$ in **1** and the formation of $\Delta^{10,11}$ in **HTT12-1** (16) (Table 1, Figure S1-6).

188   The planner structure of **HTT12-1** was further established by detailed interpretation of its 2D

189   NMR spectra. Four spin systems (C-2–C-13, C-16–C-13–C-14–C-15, C-6–C-5–C-18, and C-9–C-

190   19) as depicted in Figure S6 were established based on the ^1H–^1H COSY spectrum. These fragments,

191   ester or amide carbonyl groups, tetrasubstituted double bond, tertiary methyl, and the oxygenated or

192   nitrogenated methines were further linked by the HMBC spectrum from H-2 to C-12, H_3-17 to C-

193   10/C-11/C-12, H-9 to C-10/C-20, H_2-19 to C-10/C-21/C-25, H-5 to C-3/C-7, H-6 to C-1'/C-7, and H-

194   4' to C-1', which generated a monocycle ring system. Especially, the key HMBC correlations from

195   H-9, H_3-17 and H_2-19 to C-10, and from H-2 and H_3-17 to C-12, combined with the downfield-

196   shifted chemical shift of C-10 (δ_C 175.4) and upfield-shifted chemical shift of C-2 (δ_C 76.6), revealed

197   the enolic hydroxy group and 1-methylpropyl group at C-10 and C-2, respectively. Thus, the gross

198   structure of HTT12-1 was established (Figure 1). The relative configurations of HTT12-1 was

199   assigned to be the same as pyridomycin by comparing their 1D NMR data, while the relative

200   configurations of C-2 and C-13 were not determined. We therefore named compound **HTT12-1** as

201   pyridomycin B (**4**) for the similar scaffold with pyridomycin.

Determination of Pyr2 active sites

203   Pyridomycin B featured with enol moiety in pyridyl alanine moiety and a saturated 3-

204   methylvaleric acid group. Inspired by the chemical structure of pyridomycin B, we reexamined the

205   role of Pyr2. The classical SDRs family is known for sharing the canonical NAD(P)-binding motif,

206   and this glycine-rich region plays a critical role in domain stability as well as allows access of the

207   NAD(P) pyrophosphate. Comparison of the primary sequences of Pyr2 and its homologues revealed

208   TGGxxGxG, the highly conserved Rossmann fold of classical SDR subfamily. In most representative

209   3-ketoacyl-ACP reductases, the three conserved active residues are Ser-Tyr-Lys (27). Tyr residue

210   acts as a catalytic acid/base which forms a hydroxyl-tyrosinate ion that donates or abstracts a proton

211   from the substrate (26). Intriguingly, alignment of Pyr2 with other canonical SDR family

212   oxidoreductases reveals that Pyr2 contains a His instead of the usually conserved Tyr such that the

213   active site triad is S140-H154-K158 (Figure 2).

214   Since the active triad S-H-K in Pyr2 is different from the conserved catalytic triad of typical

215   SDR family proteins, we performed site-directed mutagenesis to probe the functions of the three key

216   residues. Encouraged by the successful complementation of mutant HTT12 with Pyr2, we mutated

217   these residues to Ala respectively using pJTU4659 as template to test *in vivo* if these Pyr2 variants

218   retained the ability of pyridomycin B production. The resulting plasmids containing *pyr2* with point

219   mutation were introduced into HTT12 mutant by conjugation for complementation. Pyridomycin and

220   pyridomycin B showed some different MS/MS fragmentation patterns, we therefore chose extracted

221   ion chromatograms (EIC) of fragment *m/z* 411 and *m/z* 409, respectively for comparison. After

222   carefully analyzing the MS/MS profile, we found that mutating of the His154 residue to Alanine

223   (Pyr2/H154A) cannot restore the production of pyridomycin. Both of the Pyr2/S140A and

224   Pyr2/K158A mutant exhibit the fragment *m/z* 411, which means the complementation of pyridomycin

225   production. Moreover, we mutated the His154 to Tyr and identified that Pyr2/H154Y mutant endow

226   the capability of pyridomycin production (Figure 4). Such observations suggest that the catalytic triad

227   engages in a different manner and His154 is critical for the function of Pyr2.

228

229   **Discussion**

230   Tuberculosis (TB) is one of the world's leading causes of death. Since the discovery of pyridomycin

231   as the antituberculous natural product over 60 years ago, it hasn't garnered considerable attention

232   until being demonstrated as a target inhibitor of InhA enoyl reductase of *Mtb* (28). Recently,

233   significant progress in understanding the antituberculous mechanism inspired generation of a serious

234   pyridomycin derivatives for SAR studies (13-15, 24). Generating pyridomycin analogues by genetic

235   manipulation is an alternative approach based upon understanding of the biosynthetic mechanisms. In

236   this work, we report the characterization of a new pyridomycin analogue from a *pyr2* knockout

237   mutant HTT12, which lays a foundation for utilization of the pyridomycin pathway to develop

238   promising antituberculous derivatives by genetic engineering.

239   Pyr2 is a 3-ketoacyl-ACP reductase, which belongs to the SDR superfamily. The draft genome

240   sequence analysis of *S. pyridomyceticus* revealed the presence of additional three Pyr2 homologues

241   (Figure S7) with >90% coverage of varying homology (>30% identities, ~52% similarities).

242   Although the overall structure of Pyr2 and SDR proteins are highly analogous, the catalytic

243   conformation of Pyr2 may diverge from other classical SDR family oxidoreductases as the variation

244   of the active site triad. In addition, Δ*pyr2* mutant HTT12 lost the productivity of pyridomycin,

245   showing that these homologues could not restore the function of Pyr2. It clearly indicates that Pyr2 is

246   pathway specific for pyridomycin biosynthesis.

247   Previous biosynthetic analysis revealed that among the NRPS-PKS assembly line of pyridomycin,

248   PKS module PyrF (KS-AT-MT-ACP) incorporates the propionic acid derived unit. According to the

249   chemical structure of final product, there is a requirement for the reduction of C-10 keto of the linear

250   peptide-polyketide intermediate. Notably, the PKS PyrF lacks a KR domain for hydroxyl group

251   formation, in contradiction to the presence of hydroxyl group (*) at C-10 of pyridomycin. Several

252   examples of standalone ketoreductase from assembly-line system have been reported. For example,

253   AntM perfroms a ketoreduction of the C-8 carbonyl of the linear ACP-bound intermediate in

254   antimycin pathway (22). SimC7 is a ketoreductase that reduces the carbonyl to a hydroxyl group at

255   the C-7 position in simocyclione D8 (23). It may hint that the Pyr2 contributes to the formation of the

256   C-10 hydroxyl group. *In vivo* knockout of *pyr2* accumulated a new pyridomycin analogue,

257   pyridomycin B. Although pyridomycin B specifically featured the enoyl group at C-10–C-11, we

258   speculated that the enol form presented as the major species in equilibrium instead of the keto form

259   due to the bulky aryl group of pyridomycin B at C-9 and dicarbonyl at C-10 and C-12. Isolation of

260   pyridomycin B implies that Pyr2 functions as a *trans* ketoreductase, acts upon an acyl carrier protein-

261   bound linear biosynthetic intermediate and catalyzes the formation of hydroxyl group on C-10 (*)

262   prior to TE-catalyzed cyclization. We also purified Pyr2 protein and carried out *in vitro* experiment

263   using pyridomycin B as the substrate. Unfortunately, no detectable new product in the reaction

264   indicated that Pyr2 catalyzes a reaction on ACP or PCP-tethered substrate (data not show).

265   The enolic acid moiety of pyridomycin is essential for antibiotic activity, interacting with the

266   substrate binding pocket and resulting in competitive inhibition (29). Synthesis of the enol moiety is

267   also an obstacle in *de novo* synthesis of pyridomycin. Pyridomycin B harbors a saturated 3-

268   methylvaleric acid group rather than an enol moiety. Based on the structure of pyridomycin B, along

269   with the fact that there is no other dehydrogenase within this gene cluster, it seems that Pyr2 is also

270   responsible for the double bond (C-2, #) formation in the isoleucine-derived moiety. We then

271   proposed that the NAD(P) dependent enzyme Pyr2 may act as a bifunctional enzyme that abstracts

272   the hydrogen from the α-hydroxyl-β-methylvaleric acid moiety of PyrG-tethered linear NRP/PK

273   chain for NAD(P)H formation, and then uses the NADPH formed in situ to reduce the β-keto (*) to

274   generate a hydroxyl group (Figure 5), suggesting an atom economy manner.

275   In summary, we confirmed that Pyr2, a 3-oxoacyl ACP reductase is essential for pyridomycin

276   biosynthesis. The varied catalytic triad of Pyr2 suggests that the function of Pyr2 is different from the

277   typical SDRs. The isolated pyridomycin B from the mutant Δ*pyr2* supports a biosynthetic model that

278   Pyr2 converts the keto group to the hydroxyl group of pyridyl alanine moiety and forms the double

279   bond of the 2-hydroxy-3-methylpent-2-enoic acid moiety using an atom economy and synergistic

280 strategy. The enoic acid moiety is known to be an important pharmacophoric group in pyridomycin.

281 Studies in future including functional characterization and structural elucidation of Pyr2 will lead to

282 defining the essential motif and major active-residues of Pyr2 for interacting with the substrate,

283 which would help to introduce other enol carboxylic acids to expand structural diversity of

284 pyridomycin by engineering Pyr2 for antimycobacterial activity screening.

285 **Materials and Methods**

286 **Bacterial strains, plasmids, and culture conditions**

287 Bacterial strains, plasmids and oligo primers for PCR amplification used in this study are

288 summarized in Table 2-3. PCRs were performed using rTaq (Takara biotechnology, Dalian, China)

289 or KOD (Toyobo, Japan), and the PCR primers were synthesized by Invitrogen (Shanghai, China).

290 Overlapping-PCR based site-directed mutagenesis was employed to introducing point mutations of

291 *pyr2*. Restriction endonucleases were purchased from Thermo Fisher and the reactions were

292 performed according to the manufacture's procedures. Other common biochemical, chemical

293 solvents and media components were purchased from standard commercial sources and used directly.

294 *E. coli* strains were routinely grown in LB medium at 37°C and supplemented with appropriate

295 antibiotics for plasmid maintenance. *Streptomyces pyridomyceticus* and the derived mutants were

296 cultured in liquid tryptic soy broth (TSB) for mycelium, on solid COM medium for sporulation, on

297 2CM medium for conjugation and in fermentation medium (2.5% glucose, 1.5% soybean meal, 0.5%

298 NaCl, 0.05% KCl, 0.025% $MgSO_4 \cdot 7H_2O$, 0.3% K_2HPO_4, 0.3% $Na_2HPO_4 \cdot 12H_2O$, pH 7.2) for

299 production of pyridomycin and pyridomycin B. *E. coli-Streptomyces* conjugations were performed

300 following previously reported protocols (30).

301 **DNA sequencing and bioinformatics analysis**

302 The draft genome was submitted to secondary metabolite gene cluster analysis using antiSMASH

303 (31). A PSI-BLAST search of the NCBI nonredundant homology search was conducted on the *pyr2*

304 and a tblastn search performed by BioEdit. The NRPS and PKS architectures were predicted by

305 NRPS-PKS predictor (http://nrps.igs.umaryland.edu/) and confirmed against GenBank database by

306 BLAST by manual inspection. Multiple sequence alignments and local blast analysis were performed

307 using BioEdit Sequence Alignment Editor. The Pyr2 sequence was aligned with ClustalW using

308 BioEdit and phylogenetic analyses were performed by MEGA-X with 1000 bootstrap replications

309 (32). Using Pyr2 as the query, we searched for homologous proteins in the nonredundant database of

310 Genbank and create the sequence similarity networks (SNN) using Enzyme Function Initiative (EFI)

311 tools (33, 34). Cytoscape V6.0 was used for the SNN visualization and analysis.

312 **Complementation of Δ*pyr2* mutant HTT12**

313 In *pyr2* inactivation mutant *S. pyridomyceticus* HTT12, the *pyr2* was replaced by kanamycin

314 resistance cassette using a standard λRed-mediated PCR targeting recombination system. For the

315 construction of the gene complementation construct, *pyr2* was amplified from *S. pyridomyceticus*

316 genomic DNA by PCR using high-fidelity DNA polymerase and digest with *Nde*I-*Eco*RI. The

317 resulting fragment was cloned downstream of the *PermE** promoter into pIB139, the *E. coli-*

318 *Streptomyces* expression shuttle vector, digested with the corresponding restriction enzymes to yield

319 the complementary plasmid pJTU4656 (Table S1). To achieve the point mutations in Pyr2,

320 pJTU4656 (H154Y), pJTU4656 (H154A), pJTU4656 (S154Y), and pJTU4656 (K154Y) were

321 constructed by site-directed mutagenesis using the primers listed in Table 2. The plasmid pJTU4656

322 and its derivatives carrying point mutations in *pyr2* were introduced into mutant HTT12 respectively

323 by intergeneric conjugation as previously described. The resultant mutant strains were selected for

324 using kanamycin resistance.

Fermentation, production, and HPLC analysis of pyridomycin and derivatives

325

326   The Δ*pyr2* mutant HTT12 were cultured following previously reported procedures (24), with the wild

327   type producer as a control. The seed culture was prepared by inoculating 25 mL of TSB medium in

328   250 mL flask with fresh spore from COM agar plate and incubating at 30°C for 24h on a rotary

329   shaker (220 rpm). The seed culture was inoculated into a fermentation medium at 5%, and continued

330   to incubate for 3 days. The fermentation broth was extracted three times with ethyl acetate, and the

331   combined extract was concentrated in a vacuum evaporator to generate a solid residue. The resulting

332   residue was dissolved in 1 mL methanol, centrifuged and filtered prior to analysis. HPLC-MS

333   analysis was performed on a ZORBAX RX-C18 column (150×4.6 mm, 5 μm, Agilent). The column

334   was first equilibrated with 80% solvent A (0.1% formic acid in water) and 20% solvent B (0.1%

335   formic acid in acetonitrile). After 5 min of isocratic flow, a linear gradient was developed with a 25-

336   min linear gradient from 20% B to 80% B at a flow rate of 0.5 mL/min and UV detection at 305 nm.

337   The mass spectrometer was run in positive ion detection mode and set to scan between 100 and 800

338   *m/z*.

Isolation and structure elucidation of pyridomycin B

339

340   Large-scale fermentation (19 L) was carried out to isolate sufficient quantities of metabolite from the

341   Δ*pyr2* mutant HTT12 for structural elucidation. The supernatant was separated from mycelia by

342   centrifugation (8000 rpm, 15 min), and was extracted three times with 10 L of ethyl acetate (EtOAc).

343   The organic solvent in the combined extracts were removed under reduced pressure. The resulted

344   crude extract (4.28 g) was adsorbed to 200 g RP-18 reverse phase resin (YMC group, Japan) and was

345   eluted with a gradient of CH_3OH-H_2O (20:80, 30:70, 50:50, 70:30 and 100:0) at 3 mL/min to give

346   120 fractions. Each fraction was tested for alkaloid compounds by bismuth potassium iodide solution.

347   Fractions with positive signals (fraction 69-83) were combined and concentrated to give 120 mg Fr2,

348   further purified by a Sephadex LH-20 column using MeOH as the mobile phase at 1 mL/min to give

349   a subfraction Fr2A (15 mg) with positive signals by TLC and UV detection. Fraction Fr2A was

350   purified by silica gel column chromatography using gradient of H_2O/CH_3OH (70:30, 40:60) at 2

351   mL/min to yield Fr2A1 25 mg, and then subjected to semipreparative preparative HPLC (ZORBAX

352   Eclipse XDB-C18, 9.4 × 250 mm, 5 μm, Agilent) using 0.1% formic acid in water/CH_3OH as the

353   mobile phase to afford pyridomycin B (25 mg).

354   NMR spectra were recorded on a Bruker AV-III 600 (500 MHz) spectrometer. Chemical shifts are

355   reported in parts per million (ppm) and coupling constants *J* are given in Hertz (Hz). Structural

356   elucidation of the isolated compounds was achieved by means of 1D (^{1}H and ^{13}C) and 2D (^{1}H-^{1}H

357   COSY, HSQC, and HMBC) NMR spectra (Figure S1-S6) and by comparison of the spectra with

358   published data (16). The NMR data are summarized in Table 3. Samples were dissolved in CD_3OD.

359   High resolution MS analysis was performed on an Agilent 1200 series LC/MSD trap system in

360   tandem with a 6530 Accurate-Mass Q-TOF mass spectrometer with an ESI source (50-800 *m/z* mass

361   range at positive mode).

Antimicrobial activity assay

363   The antimycobacterial activities of the pyridomycin producers against indicator strain

364   *Mycobacterium smegmatis* mc^{2}155 using a standard diffusion assay. The 20 μL crude extracts of *S.*

365   *pyridomyceticus* strains were dropped on paper disks and placed on the solid LB agar plates

366   containing ~10^7 *M. smegmatis* mc^{2}155 cell. The plates were incubated overnight at 37°C and halo

367   zone of inhibition were observed. Pyridomycin was used a positive control.

SUPPLEMENTAL MATERIAL

369   Supplemental File including supplemental figure 1-7.

ACKNOWLEDGMENTS

References

1. WHO. 2018. 2018 Global tuberculosis report. World Health Organization Press W, Geneva, Switzerland

2. Lechartier B, Rybniker J, Zumla A, Cole ST. 2014. Tuberculosis drug discovery in the post-post-genomic era. EMBO Mol Med 6:158-68.

3. Dong M, Pfeiffer B, Altmann KH. 2017. Recent developments in natural product-based drug discovery for tuberculosis. Drug Discovery Today 22:585-591.

4. Herrmann J, Rybniker J, Muller R. 2017. Novel and revisited approaches in antituberculosis drug discovery. Curr Opin Biotechnol 48:94-101.

5. Baptista R, Bhowmick S, Nash RJ, Baillie L, Mur LA. 2018. Target discovery focused approaches to overcome bottlenecks in the exploitation of antimycobacterial natural products. Future Med Chem 10:811-822.

6. Riccardi G, Pasca MR. 2014. Trends in discovery of new drugs for tuberculosis therapy. J Antibiot (Tokyo) 67:655-659.

7. Pan P, Tonge PJ. 2012. Targeting InhA, the FASII Enoyl-ACP Reductase: SAR Studies on Novel Inhibitor Scaffolds. Current Topics in Medicinal Chemistry 12:672-693.

8. Rozman K, Sosic I, Fernandez R, Young RJ, Mendoza A, Gobec S, Encinas L. 2017. A new 'golden age' for the antitubercular target inha. Drug Discovery Today 22:492-502.

9. Vilcheze C, Jacobs WR, Jr. 2007. The mechanism of isoniazid killing: clarity through the scope of genetics. Annu Rev Microbiol 61:35-50.

10. Hartkoorn RC, Sala C, Neres J, Pojer F, Magnet S, Mukherjee R, Uplekar S, Boy-Rottger S, Altmann KH, Cole ST. 2012. Towards a new tuberculosis drug: pyridomycin - nature's isoniazid. Embo Molecular Medicine 4:1032-1042.

11. Maeda K, Kosaka H, Okami Y, Umezawa H. 1953. A new antibiotic, pyridomycin. J Antibiot (Tokyo) 6:140.

12. Ogawara H, Maeda K, Umezawa H. 1968. The biosynthesis of pyridomycin. I. Biochemistry 7:3296-3302.

13. Hartkoorn RC, Pojer F, Read JA, Gingell H, Neres J, Horlacher OP, Altmann KH, Cole ST. 2014. Pyridomycin bridges the NADH- and substratebinding pockets of the enoyl reductase InhA. Nature Chemical Biology 10:96-98.

14. Horlacher OP, Hartkoorn RC, Cole ST, Altmann KH. 2013. Synthesis and Antimycobacterial Activity of 2,1'-Dihydropyridomycins. Acs Medicinal Chemistry Letters 4:264-268.

15. Kienle M, Eisenring P, Stoessel B, Horlacher OP, Hasler S, van Colen G, Hartkoorn RC, Vocat A, Cole ST, Altmann KH. 2020. Synthesis and Structure-Activity Relationship Studies of C2-Modified Analogs of the Antimycobacterial Natural Product Pyridomycin. J Med Chem 63:1105-1131.

16. Kinoshita M, Nakata M, Takarada K, Tatsuta K. 1989. Synthetic Studies of Pyridomycin .5. Total Synthesis of Pyridomycin. Tetrahedron Letters 30:7419-7422.

17. Wash CT, Tang Y. 2017. Natural Product Biosynthesis: Chemical Logic and Enzymatic Machinery. Royal Society of Chemistry, CPI Group (UK) Ltd, Croydon, CR04YY, UK.

18. Piel J. 2010. Biosynthesis of polyketides by trans-AT polyketide synthases. Natural Product Reports 27:996-1047.

19. Helfrich EJN, Piel J. 2016. Biosynthesis of polyketides by trans-AT polyketide synthases. Natural Product Reports 33:231-316.

20. Heneghan MN, Yakasai AA, Williams K, Kadir KA, Wasil Z, Bakeer W, Fisch KM, Bailey AM, Simpson TJ, Cox RJ, Lazarus CM. 2011. The programming role of trans-acting enoyl reductases during the biosynthesis of highly reduced fungal polyketides. Chemical Science 2:972-979.

21. Zou Y, Yin H, Kong D, Deng Z, Lin S. 2013. A trans-acting ketoreductase in biosynthesis of a symmetric polyketide dimer SIA7248. Chembiochem 14:679-683.

22. Fazal A, Hemsworth GR, Webb ME, Seipke RF. 2021. A Standalone beta-Ketoreductase Acts Concomitantly with Biosynthesis of the Antimycin Scaffold. ACS Chem Biol 16:1152-1158.

23. Schafer M, Stevenson CEM, Wilkinson B, Lawson DM, Buttner MJ. 2016. Substrate-Assisted Catalysis in Polyketide Reduction Proceeds via a Phenolate Intermediate. Cell Chem Biol 23:1091-1097.

24. Huang TT, Wang YM, Yin J, Du YH, Tao MF, Xu J, Chen WQ, Lin SJ, Deng ZX. 2011. Identification and Characterization of the Pyridomycin Biosynthetic Gene Cluster of Streptomyces pyridomyceticus NRRL B-2517. Journal of Biological Chemistry 286:20648-20657.

25. Huang TT, Li LL, Brock NL, Deng ZX, Lin SJ. 2016. Functional Characterization of PyrG, an Unusual Nonribosomal Peptide Synthetase Module from the Pyridomycin Biosynthetic Pathway. Chembiochem 17:1421-1425.

26. Kavanagh K, Jornvall H, Persson B, Oppermann U. 2008. The SDR superfamily: functional and structural diversity within a family of metabolic and regulatory enzymes. Cellular and Molecular Life Sciences 65:3895-3906.

442 27. Filling C, Berndt KD, Benach J, Knapp S, Prozorovski T, Nordling E, Ladenstein R, Jornvall
443   H, Oppermann U. 2002. Critical residues for structure and catalysis in short-chain
444   dehydrogenases/reductases. J Biol Chem 277:25677-25684.

445 28. Wright GD. 2012. Back to the future: a new 'old' lead for tuberculosis. Embo Molecular
446   Medicine 4:1029-1031.

447 29. Hartkoorn RC, Pojer F, Read JA, Gingell H, Neres J, Horlacher OP, Altmann KH, Cole ST.
448   2014. Pyridomycin bridges the NADH- and substrate-binding pockets of the enoyl reductase
449   InhA. Nat Chem Biol 10:96-98.

450 30. Kieser T, Bibb, M. J., Chater, K. F., Butter, M. J., and Hopwood, D. 2000. Practical
451   Streptomyces Genetics: A Laboratory Manual. John Innes Foundation, Norwich, UK.

452 31. Blin K, Shaw S, Steinke K, Villebro R, Ziemert N, Lee SY, Medema MH, Weber T. 2019.
453   antiSMASH 5.0: updates to the secondary metabolite genome mining pipeline. Nucleic Acids
454   Research 47:W81-W87.

455 32. Kumar S, Stecher G, Li M, Knyaz C, Tamura K. 2018. MEGA X: Molecular Evolutionary
456   Genetics Analysis across Computing Platforms. Mol Biol Evol 35:1547-1549.

457 33. Gerlt JA. 2017. Genomic Enzymology: Web Tools for Leveraging Protein Family Sequence-
458   Function Space and Genome Context to Discover Novel Functions. Biochemistry 56:4293-
459   4308.

460 34. Gerlt JA, Bouvier JT, Davidson DB, Imker HJ, Sadkhin B, Slater DR, Whalen KL. 2015.
461   Enzyme Function Initiative-Enzyme Similarity Tool (EFI-EST): A web tool for generating
462   protein sequence similarity networks. Biochim Biophys Acta 1854:1019-1037.

463

464

465 **TABLE 1** [1]H (500 MHz) and ^{13}C (125 MHz) NMR data of **pyridomycin B** (δ in ppm).

position	$\delta_H{}^b$, multi (J in Hz)	δ_C, type	position	$\delta_H{}^b$, multi (J in Hz)	δ_C, type
2	4.06, d (4.5)	76.6, CH	18	1.38, d (7.0)	18.5, CH$_3$
3		175.2 ^{c}, C	19	3.58, dd (14.0, 4.0)	32.7, CH$_2$
				3.18, dd (14.0, 2.5)	
5	5.57, m	71.5, CH	20		133.1, C
6	5.88, m	57.3, CH	21	7.56, brd (7.5)	141.1, CH
7		169.8, C	22	7.34, dd (7.5, 5.0)	125.4, CH
9	4.61, brs	60.5, CH	23	8.39, dd (5.0, 1.0)	148.0, CH
10		175.4 ^{c}, C	25	8.22, d (1.5)	150.2, CH
11		103.4, C	1′		170.9, C
12		174.3, C	2′		132.5, C
13	1.86, m	40.4, CH	3′		159.5, C
14	1.54, m	25.2, CH$_2$	4′	7.41, brd (8.5)	127.7, CH
15	0.96, t (7.5)	12.4, CH$_3$	5′	7.51, dd (8.5, 4.0)	130.8, CH
16	1.00, d (7.0)	16.0, CH$_3$	6′	8.19, d (4.0, 1.0)	141.5, CH
17	1.53, s	5.7, CH$_3$			

466   ^{a}. in CD$_3$OD. ^{b}.“m” means overlapped or multipet with other signals. ^{c}. may be interchanged in each

467   column.

468

469 **TABLE 2 Plasmids and posmids used in this study.**

Strains	Relevant phenotype	Source/References
Streptomyces pyridomyceticus		
NRRL B-2517	Wild type producer of pyridomycin	ARS Culture Collection
HTT12	*S. pyridomyceticus* mutant with *pyr2* gene deletion by PCR targeting strategy, kanamycin resistance	
HTT12::pJTU4656	HTT5 complemented with pJTU4656 harboring full length of *pyr2*, apramycin and kanamycin resistance	This work
Escherichia coli		
DH10B	*E. coli* host for general cloning [F⁻ *mcrA* Δ(*mrr- hsdRMS-mcrBC*)*φ80dlacZ* Δ*M15* Δ*lacX74 deoR recA1 endA1 ara* Δ139 D (*ara,leu*)1697 *galU galK* λ⁻ *rspL nupG*]	
ET12567/pUZ8002	Methylation-deficient *E. coli* host for intergeneric conjugation [*rec*F, *dam*⁻, *dcm*⁻, *hsd*S, Cml^R, Km^R]	
BW25113/pIJ790	*E. coli* host for λRED-mediated PCR targeting	
Plasmids		
pIB139	*aac(3)IV*, int, attΦC31, reppuc,oriT, PermE	
Cosmid 3C10	An end-sequenced cosmid which contains partial pyridomycin biosynthetic gene cluster	This study
3C10pyr2-kan	The *pyr2* in cosmid 13C6 substituted using the PCR-targeting method by kanamycin cassette which amplified with primers Pyr2tgtF and Pyr2tgtR	(24)
pJTU4656	The PCR amplified *pyr2* from cosmid 3C10 was cloned into the NdeI and EcoRI site of pIB139	(24)
pJTU4656-H154Y	Site-directed mutagenesis of histidine(154) to tyrosine in *pyr2* by overlapping PCR using pJTU4656 as template	This study
pJTU4656-H154A	Site-directed mutagenesis of histidine(154) to alanine in *pyr2* by overlapping PCR using pJTU4656 as template	This study
pJTU4656-S140A	Site-directed mutagenesis of serine (140) to alanine in *pyr2* by overlapping PCR using pJTU4656 as template	This study
pJTU4656-K158A	Site-directed mutagenesis of lysine (158) to alanine in *pyr2* by overlapping PCR using pJTU4656 as template	This study

470

471 **TABLE 3 Primers used in this study**

| Primers	Sequence
Pyr2tgtF	ATGACTCTTTCGCAGAAGAAGGCGCTGGTCACCGGAGGCATTCCGGGGATCCGTCGACC
Pyr2tgtR	TCAGACCATGCCGCCGGTCACGCGCAGGTTCTGGCCGCTTGTAGGCTGGAGCTGCTTC
Pyr1&2IDF	GTGCCGACCGACCGCAACCG
Pyr1&2IDR	TCAGACCATGCCGCCGGTCAC
Pyr2expNF	GGCAATTCCATATGACTCTTTCGCAGAAGAA
Pyr2expER	GGAATTCTCAGACCATGCCGCCGGTC
Pyr2-H154Y-F	GTGTCGCTGTACGCCGGCAGCAAGGCG
Pyr2-H154Y-R	GCTGCCGGCGTACAGCGACACGCCGGG
Pyr2-H154A-F	GTGTCGCTGGCCGCCGGCAGCAAGGCG
Pyr2-H154A-R	GCTGCCGGCGGCCAGCGACACGCCGGG
Pyr2-S140A-F	ATCAACCTCGCGACCGCCAACACCGTG
Pyr2-S140A-R	GTTGGCGGTCGCGAGGTTGATGATGCG
Pyr2-K158A-F	GCCGGCAGCGCGGCGGCCGTCGAGCAG
Pyr2-K158A-R	GACGGCCGCCGCGCTGCCGGCGTGCAG

472

1
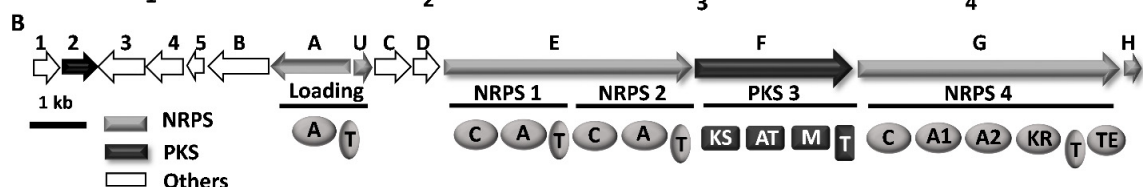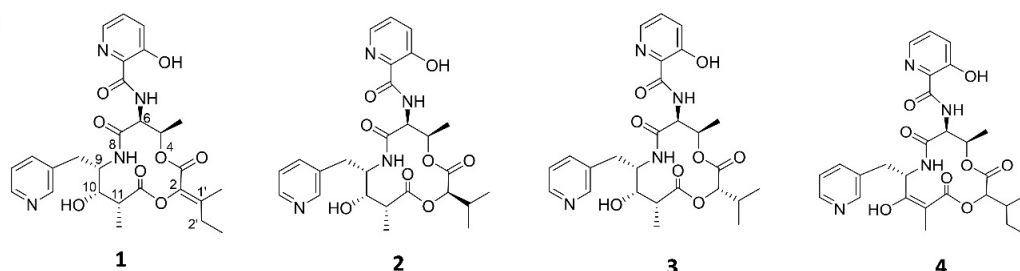
Figure 1. In vivo characterization of *pyr2* in pyridomycin biosynthesis. A. Structures of

pyridomycin and pyridomycin B; B. Genetic organization of the pyridomycin biosynthetic gene cluster

from *S. pyridomyceticus* B2517. Pyr2 is highlighted in black.

5

6

7

8
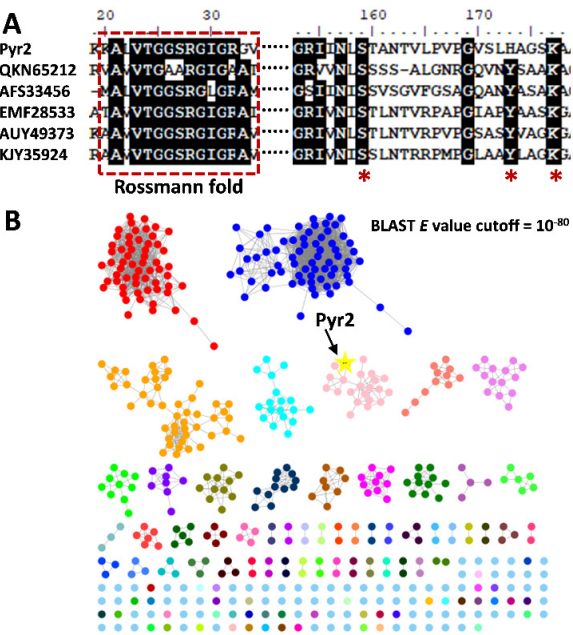
Figure 2. Bioinformatics analysis of Pyr2. A. Sequence alignment of selected Pyr2 homologs. The rossmann fold is highlighted in dash. The catalytic residues are shown with asterisks (*). B. A sequence similarity network (SSN) of Pyr2 homologs (sequence identity of >40%) visualized by Cytoscape.

12
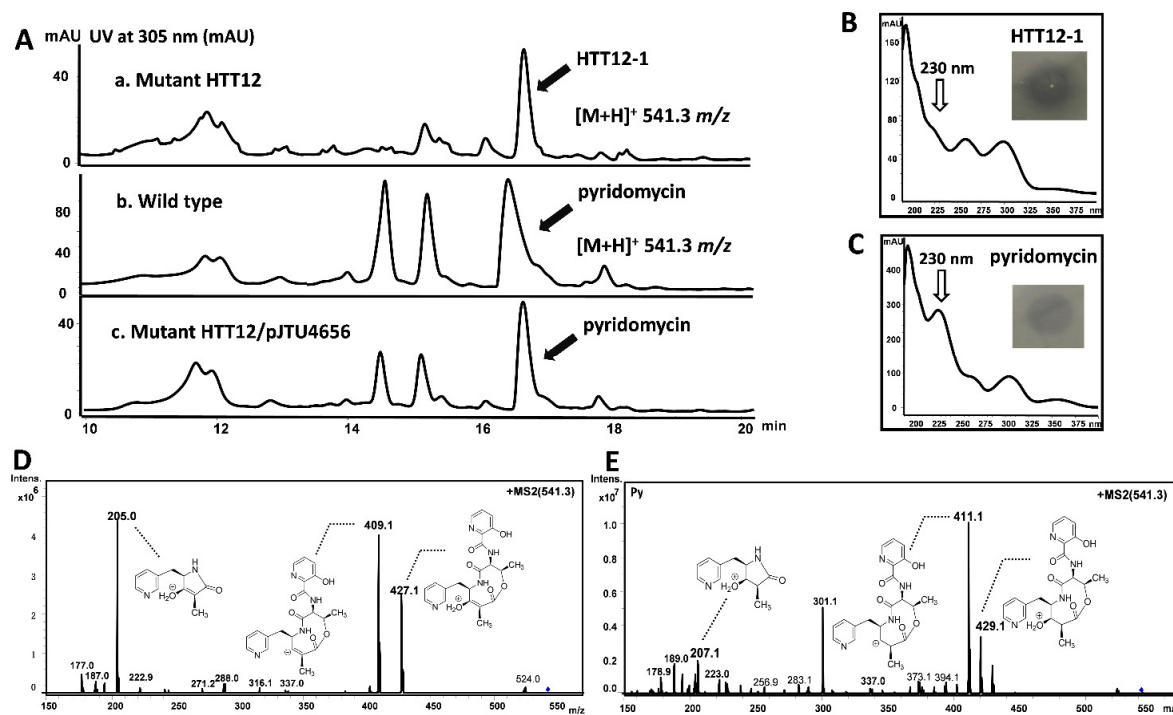
Figure 3. In vivo characterization of *pyr2* in pyridomycin biosynthesis. A. UV at 305 nm from HPLC analysis of metabolites from wild type *S. pyridomyceticus* B2517, HTT12 (Δ*pyr2*) and HTT12::*pyr2*. B. Bioassay against *M. smegmatis* mc^{2}155 and UV spectrum of the peak from HTT12, pyridomycin as a control (C); MS/MS spectrum of the peak from HTT12 (D) and pyridomycin (E), respectively.

19
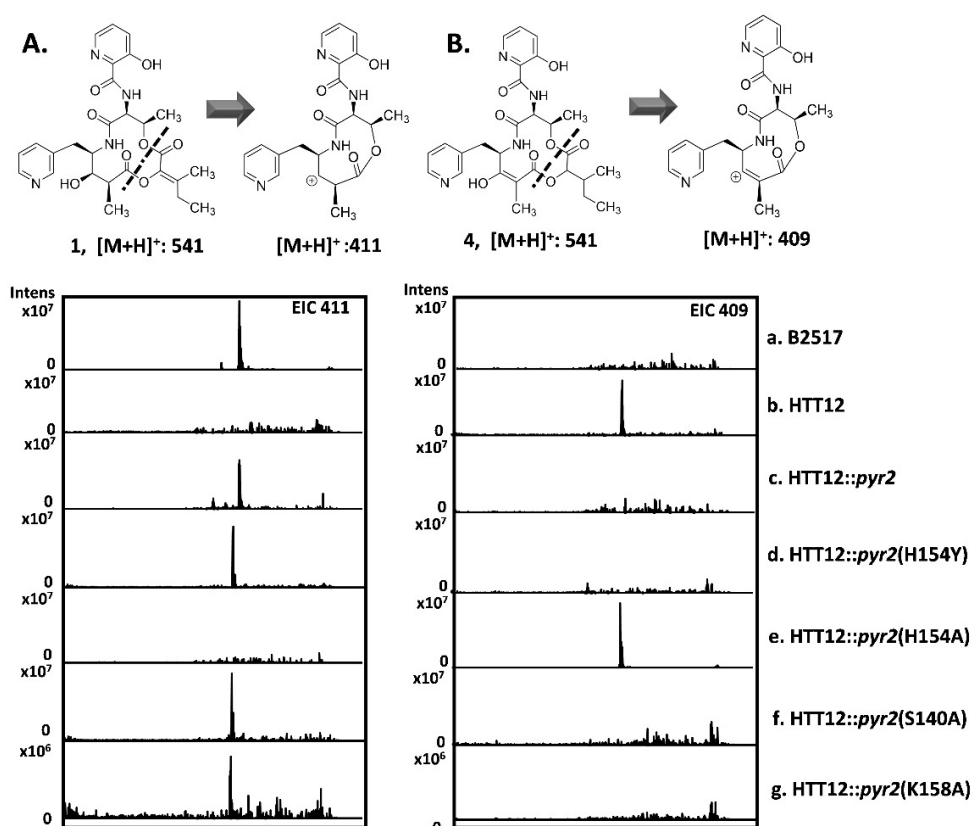
Figure 4. LC-MS analysis of *S. pyridomyceticus* recombinant strains. Extracted ion chromatograms (EIC, *m/z* at 409 and 411) from LC-MS analysis of metabolites from *S. pyridomyceticus* recombinant strains. The detection of each strain was individually scanned by using MS/MS fragmentation patterns of *m/z* 409 for pyridomycin and 411 for pyridomycin B.
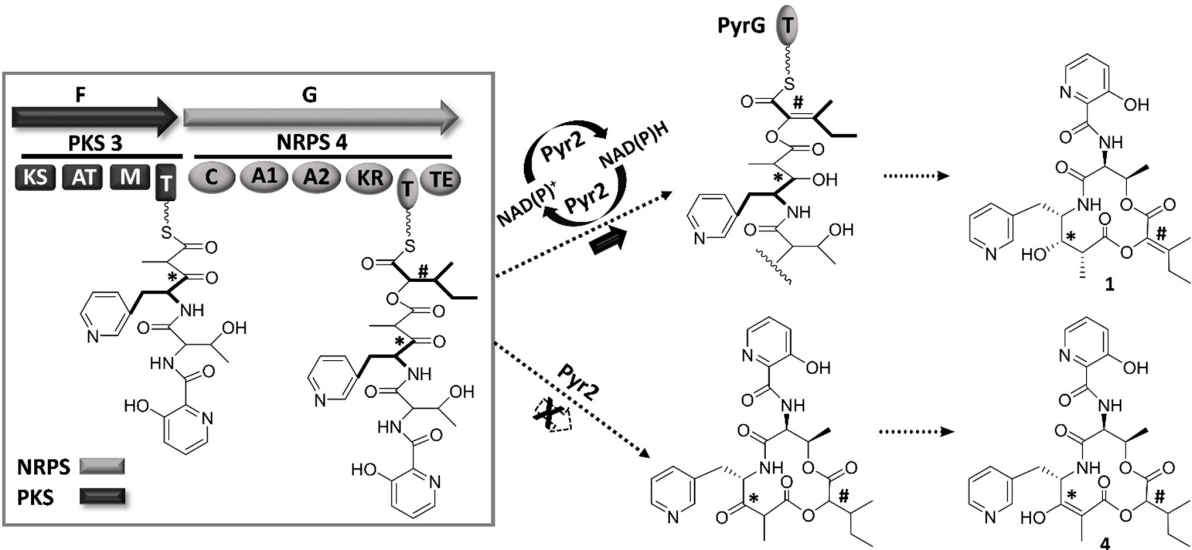
Figure 5. Proposed biosynthesis of pyridomycin supported by the isolation of pyridomycin B from *S. pyridomyceticus* mutant HTT12.